High Frequency Acoustic Signal Sensing Using Light

Chavan Aniket Laxman

A dissertation submitted for the partial fulfillment of BS-MS dual degree in Science

Department of Physical Sciences
Indian Institute of Science Education and Research
Mohali

December 2020

Certificate of Examination

This is to certify that the dissertation titled "**High Frequency Acoustic Signal Sensing Using Light**" submitted by Chavan Aniket Laxman (Reg. No. MS14187) for the partial fulfillment of BS-MS dual degree program of the institute, has been examined by the thesis committee duly appointed by the institute. The committee finds the work done by the candidate satisfactory and recommends that the report be accepted.

Dr. Sanjib Dey | Dr. Vishal Bhardhwaj | Dr. Samir Kumar Biswas (Supervisor)

Dated: December 4, 2020

Declaration

The work presented in this dissertation has been carried out by me under guidance of Dr. Samir Kumar Biswas at the Indian Institute of Science Education and Research Mohali.

This work has not been submitted in part or in full for a degree, a diploma, or a fellowship to any other university or institute. Whenever contributions of others are involved, every effort is made to indicate this clearly, with due acknowledgement of collaborative research and discussions. This thesis is a bonafide record of original work done by me and all sources listed within have detailed in the bibliography.

Chavan Aniket Laxman
(Candidate)

Dated: December 4, 2020

In my capacity as the supervisor of the candidate's project work, I certify that the above statements by the candidate are true to the best of my knowledge.

Dr. Samir Kumar Biswas
(Supervisor)

Acknowledgements

I thank my supervisor Dr. Samir Kumar Biswas for allowing me to work with him. It was a great experience to have him as a supervisor and mentor to learn from him.

I am thankful to Dr. Sriram for helpful discussions during the projects.
I would like to thank all the lab members of Bio-Nano Photonics lab Gurpreet Kuar, Amit Kumar, Sanjay Kapur, Nitin Burman, Sarvesh Thakur, Laxman Das, Vishnu, Nehal, Asif, Sumit for helping me whenever needed.

I want to thank my family for their love, support, and freedom.

I thank all of my friends Varun Birari, Himanshu Patange, Rohit Kamate, Indrajeet Tambe, Nitin Bansal, Biswjit Sheet, Shivam Mishra, and Nishant Naresh.

List of Figures

List of Tables

Contents

Dedicated to my Grandfather.

Abstract

Photoacoustic Imaging (PAI) is a newly emerging biomedical imaging technology where a non-invasive study of a biological sample is possible. This detection method of the generated photoacoustic signal requires small in size, highly sensitive acoustic sensors capable of detecting very low-pressure amplitude signal.

Traditional material-based sensors such as PVDF and its co-polymer PZT, etc., has limited bandwidth and poor signal to noise ratio(SNR). The sensitivity of This sensor changes drastically when the size of the sensing area reduces.

There is an alternative search for developing low noise, large bandwidth, and highly sensitive acoustic sensors using alternative technologies. One of the notable research directions currently evolving is the optics-based large bandwidth acoustic signal detection. In this direction, our lab 'Bio-Nano Photonics Lab in IISER Mohali' is studying a different kind of geometries to develop micron size optical element based ultrasound detector.

In this thesis, an all-optical ultrasound sensor based on Fabry-Perot Interferometer and phase modulation are proposed to detect the photoacoustic signal. Both planer and suspended membrane designs are proposed, fabricated, and experimentally shown. Chemical etching, micro-machining, dip coating techniques, and standard communication devices are used to fabricate the sensor.

Chapter 1

Introduction

1.1 Background and Motivation

1.1.1 Background

Ultrasound wave(UW) detection and imaging technology can be used in a variety of areas such as structural health monitoring, geophysical exploration ,and biomedical imaging [1] [2] [3]. UW imaging refers to using a high-frequency sound wave to scan the target and obtaining its structural information after receiving and processing its reflected back sound signal. Until now, this realization of this technology has been done with piezoelectric devices(PZT's)[4]. This PZT's transducers have high sensitivity ,but they suffer from their low acoustic impedance mismatch with liquid giving poor non-uniform frequency response. Also, all piezoelectric transducers are vulnerable to electromagnetic interference. In addition, the cost and fragility of the piezoelectric transducer element limit their application in non-destructive imaging. Optical sensor as an alternative device has been researched and developed Over the decades. In particular, fiber optics sensor have been developed with the ability to measure different physical parameters such as pressure, strain, temperature, refractive index and other quantities by measuring the change in light intensity, phase, wavelength, polarization [5] [6] [7] [8]. Compared to its electromagnetic counterpart piezoelectric and CMUTs devices, fiber optics devices provides numerous advantages.

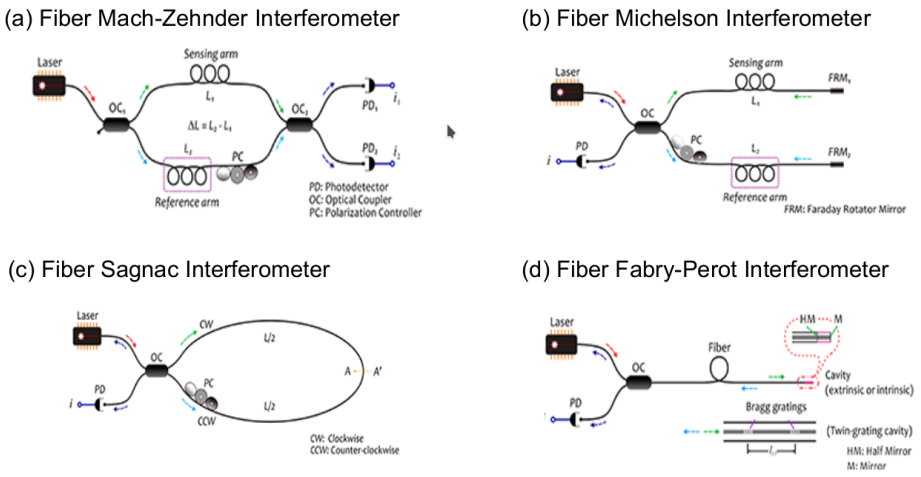

FIGURE 1.1: Configuration of types of fiber optics based interferometer sensors.

They are immune to electromagnetic interference, which makes them suitable in operation with high and varied electric field. They are made from silica glass, making them chemically and biologically inert. Also small size of optical fiber. generally on the order of hundreds of micrometer in diameter, makes the fiber optic sensor physically small and lightweight. Fiber optics sensor can perform distributed measurement and long-distance transmission enable remote sensing.

1.1.2 Fiber Optics Sensor

Fiber optic sensor exhibits inherent advantage to optical fibers. The operational principle of fiber-optic sensor is change in the characteristic of light traveling inside its core for external perturbation. The perturbation changes some of the parameters of light, either its intensity, its wavelength, its polarization state, or its optical phase. Being able to measure either of these changes makes the fiber a sensing instrument that can measure various physical parameters[3]. To achieve sensitivity different interferometric techniques are used. In Figure 1.1 are some of the widely used fiber optics sensor configuration of interferometric techniques like Mach-Zehnder, Michelson, Sagnac and Fabry-Perot interferometers are shown [9]. Fabry-Perot interferometer allows building internal cavities as well as external cavities which are sensitive to ultrasound. Ultrasound changes the optical path of these cavities, which translates into phase change in the interference signal. This kind of sensor can easily be manufactured and are

often used in distributed sensing networks. Fiber Bragg gratings can be multiplexed in wavelength on optical fiber[2] to build a distributed sensing network.

1.2 Fabry-Perot Interferometer

Perot is typically formed by two reflective mirrors or surfaces. The interference is caused by waves successively reflected between two parallel surfaces. FPI has been utilized for sensing application for a long time [10] [11]. It is capable of transferring wavelength encoded information into an intensity signal capable of fast speed sensing with high sensitivity [12]. Development of optical fiber technology, researchers realized that the combination of optical fiber sensor technology and Fabry-Perot interferometer theory could form a new type of sensor with varied advantages. The recent development in the field has enabled the FPIs to be formed on the fiber end. The Fiber tip sensors combine the advantages of both FPI sensors as well as optical fibers, including small size, high sensitivity, easy fabrication with low cost.

1.3 Photoacoustic Effect

In 1880, Alexandar Graham Bell discovered the photoacoustic effect from his observation of sound created by light [13] in various materials. Photoacoustic imaging (PA imaging) is based on the same principle. In PA imaging, a nanosecond pulse of laser light irradiates a biological sample (i.e., tissue surface, blood vessels, etc.). The light propagates into the sample, where it is scattered and absorbed by certain molecules known as chromophores. These chromophores have wavelength-dependent absorption[14]. The part of the delivered optical energy gets absorbed by the molecules and converted into heat. This leads to thermoelastic expansion of the molecules and the generation of high-frequency ultrasonic waves. This high-frequency ultrasonic wave then gets detected by an array of ultrasound detectors. Figure 1.2 shows the photoacoustic effect in the tissue structures. The detected ultrasonic waves are in the MHz frequencies ultrasound regime[15]. The pressure generated in PA imaging is in the few kPa to 100kPa range.

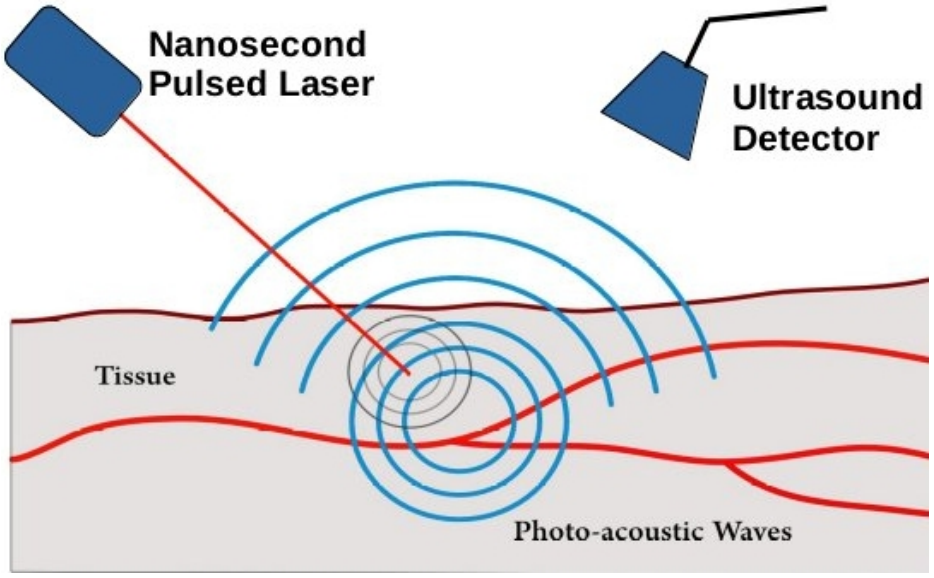

FIGURE 1.2: Photoacoustic Effect

1.4 Motivation

The use of miniature pressure sensors has been pursued in many fields, especially for medical applications, in developing minimally invasive surgical tools. These are many medical procedures benefiting from these miniature sensors [16]. Such miniature optical fiber sensors can be positioned at the tip of instrument catheters to give useful feedback during surgery.

The Fabry Perot interferometer sensor is applied in the detection of ultrasound waves generated during photoacoustic imaging. Photoacoustic imaging is a new emerging revolutionary biomedical imaging technology where non-invasive imaging of a biological sample is possible. Photoacoustic signal requires very high sensitive acoustic sensors with the capability to detect very low-pressure amplitude signals. Fiber sensors, especially Fabry Perot interferometer sensors, have already shown their potential to detect this kind of signal. A certain type of Fabry Perot interferometer sensor presented by Beard et al. is a polymer-based fiber sensor [17]. This sensor has been shown to provide wide acoustic bandwidth with uniform frequency response. Plus, the detection element volume is on the order of tens of microns. This sensor allows the photoacoustic imaging of blood vessels and superficial structures close to the surface of the tissue. To do the same thing with piezoelectric sensors, the imaging would have to be done in transmission mode, where ultrasound waves have to pass through tissue.

The transmission of the ultrasound through tissue would cause it to be attenuated, leading to a reduction in signal amplitude, which affects the final reconstructed image. Fiber optic sensors offer the prospect of overcoming most of the limitations possessed by piezoelectric transducer, especially fiber tip sensors. This sensor employs a fiber-optic down-lead to deliver light to and from the optical sensor at the end of the fiber. Theoretically, the sensitive region is defined by the spot size of the incident illumination, which is the core diameter of the fiber (typically a few microns for single-mode optical fiber). This provides us with acoustically small element sizes at frequency tens of megahertz. Other advantage includes small fiber diameter ($125um$), robustness, low cost, flexible probe-type configuration, and immunity to electromagnetic interference.

In this thesis, two different fabrication methods to make Fiber-tip sensors with the film thickness in the range of tens of micrometer was proposed. The first design implements fabricating the Fabry Perot cavity directly onto the fiber, while the second design introduces a small air cavity for the suspended membrane to be more flexible. The Young's modulus of the polymer material used is small compared to dielectrics such as SiO_2, results in larger acoustically-induced phase shifts and higher sensitivity for the sensor, making it a candidate for ultrasound testing.

1.5 Aim

Aim of the thesis include:

1. Fabricate a flexible fiber tip sensor using polymer thin film; with size as small as tens of micrometer using different thin-film fabrication techniques.
2. Study the performance of the fabricated tip sensor; for its sensitivity, stability, and linearity in ultrasound measurement.

1.6 Thesis Structure

In this thesis, a miniature optical fiber tip pressure sensor with diameter $125\mu m$ and thickness as small as tens of micrometer was fabricated with two different techniques,

and its performance under a high-frequency acoustic field has been studied. This thesis is organized into four chapters.

Chapter 1 :Introduction.This chapter covers the background and motivation of this thesis, as well as the objectives and outline of this thesis.

Chapter 2 Theory fundamentals. This chapter discusses the typical sensing setup of optical fiber sensors and their ultrasound detection mechanism.

Chapter 3 :Fabrication of fiber tip sensor. This chapter presents the fabrication steps of the sensor.

Chapter 4 Experimental setup.This chapter discusses the experimental arrangement and sensor performance under ultrasound that has been measured and analyzed.

Chapter 5 Conclusion and future work. This chapter summarizes and concludes the work done in the thesis. Also provides some suggestion on future work.

Chapter 2

Theory Fundamentals

In this chapter, the theory fundamental will be explained on the specific goals of this project. First, we will be explaining the theory behind the extrinsic Fabry-Perot interferometric sensor. This sensor will be evaluated for the detection of the acoustic signal generated from a commercially available piezoelectric transducer.

2.1 Extrinsic Fabry-Perot Interferometric Sensor

2.1.1 Principle of Operation

In a Fabry-Perot(FPI) fiber-optic interferometer, a cavity is designed so that multiply reflected light inside the cavity at a certain wavelength enter in resonance. This interferometric cavity inside the fiber can be build by placing reflective mirrors (either coating the fiber with dielectric interfaces (dielectric mirror coating, thin films, etc.) or by splicing two fibers with different core sizes and refractive indices together.
Also, this cavity can change its optical length in the presence of external perturbation (in the presence of ultrasound or thermal waves). The stress that is due to an incident acoustic wave modulates the thickness of the film, and therefore the optical phase difference between two reflections. Corresponding intensity modulation is produced, which is then transmitted back along with the fiber for detection at the photodiode. This is demodulated to obtain a measure of pressure or temperature. The scheme of common setup is shown in Figure 2.1. A fiber circulator (FC) is used to guide light from the

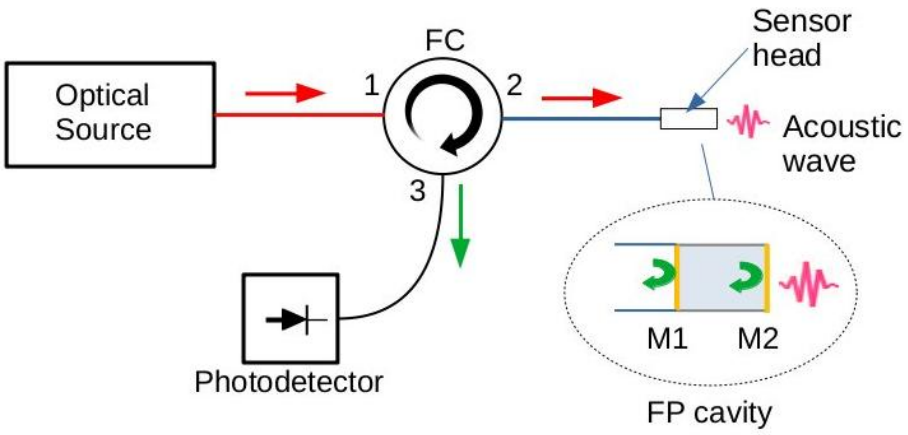

FIGURE 2.1: Schematic diagram showing the optical fiber detection of ultrasound

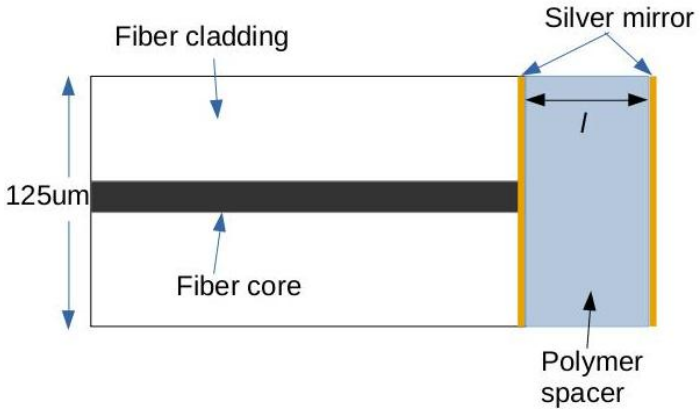

FIGURE 2.2: Schematic of FPI sensor head

broadband optical source to the interferometric cavity (red arrows) and to avoiding back reflection on the optical source. After reaching the cavity, light splits into reflected and transmitted beam at the first mirror (M1). The transmitted beam inters the cavity where it multiple reflects between the first mirror(M1) and second mirror (M2). Mirror M1 and M2 are made from silver thin films which are designed to have a reflectance of R_1 and R_2 respectively. Multiple reflected beams at the output mirror (M1) are then guided(green arrows) back to produce an interference signal detected by a photodetecting device (PD). A schematic of the tip of the fiber FPI sensor is shown in Figure 2.2. The sensing element of FPI is made up of a thin, flexible membrane of polymer spacer sandwiched between a pair of silver mirrors.

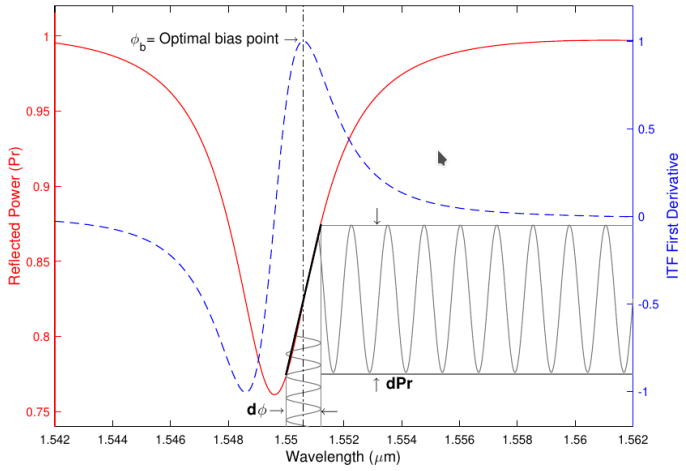

FIGURE 2.3: Interferometric Transfer Function of FPI sensor

2.1.2 Ultrasound transduction mechanism

The polymer spacer changes its thickness in proportion to the amplitude of an incident pressure wave modifying relative phase ϕ between multiple reflected beams. So, the normalized total reflected intensity $I(\phi)$ at wavelength λ allows to do a follow-up to the variation in pressure change at the output of the system. Using total reflectance equation in Fabry-Perot cavity Equation 2.1. The interferometric transfer function (ITF) of a multi-reflection interferometer with unequal mirror reflectivities R_1 and R_2 is given by

$$I(\phi) = I_0 \left(1 - \frac{(1-R_1)(1-R_2)}{(1-\sqrt{R_1 R_2})^2 + 4\sqrt{R_1 R_2}\sin^2\frac{\phi}{2}} \right) \tag{2.1}$$

where,

$$\phi = \frac{4\pi n l(p)}{\lambda} \tag{2.2}$$

I_0 is intensity of incident optical beam, λ is the optical wavelength, n and l(p) are polymer refractive index and thickness of the polymer spacer which depend upon incident acoustic pressure respectively. For plane-parallel, FPI formed with non-absorbing mirror and illumination with collimated beam the interferometric transfer function (ITF) takes the form of Airy function, shown in Figure 2.3. Here the values of reflectances of mirrors R_1 and R_2 are taken to be 75% and 99 % respectively for the sake of plotting the ITF. The dip in the ITF corresponds to destructive interference between multiply reflected beams between two mirrors. The first derivative of total reflected intensity I(ϕ) with respect to phase ϕ is

also plotted in the dashed blue line. A vertical black dashed line corresponds to the max value of the first derivative for the original ITF.

2.1.3 Sensitivity of optical FPI Sensor

2.1.3.1 Biasing the FPI sensor

The acoustic transduction mechanism for the sensor uses an optimally biased phase(ϕ_b) value. This (ϕ_b) is obtained from considering the corresponding phase to peak derivative of ITF. At this wavelength, the sensitivity and linearity are maximum. At optimally biased phase (ϕ_b), a small phase shift dϕ due to acoustic signal can be regarded as being linearly converted to a corresponding change in the reflectance I(ϕ). The sensors sensitivity and ITF is derived from Airy model. However in case of high finesse FPI cavities where mirror reflectivities are more than 90$\%$, the effect of beam divergence and non uniformity of polymer spacer can cause ITF to depart from ideal Airy model.

2.1.3.2 Optical phase sensitivity

The optical phase sensitivity is defined as the change in reflected light for small change in phase. It depends on the incident optical power and the finesse of the FPI cavity. A maximum change in reflected power dI(ϕ) occurs at maximum of derivative of Equation (2.1) with respect to ϕ. This is known as optical phase sensitivity S_0 and termed as

$$S_0 = \frac{dI(\phi)}{d\phi} \tag{2.3}$$

A high optical phase sensitivity for a sensor is achieved when small change in optical phase produce largest change in the reflected intensity. This can be achieved just by increasing the mirror reflectivities to make the slope of the reflective peak sharper.

2.1.3.3 Acoustic phase sensitivity

Acoustic sensitivity in FPI sensor is defined as modulation of optical phase dϕ produced per unit pressure dp. The change in phase arises due change in optical thickness of the

spacer. To achieve modulation of phased ϕ for a given pressure change dp, the acoustic phase sensitivity S_A can be written as

$$\frac{d\phi}{dp} = \frac{\partial\phi}{\partial l}\frac{\partial l}{\partial p} + \frac{\partial\phi}{\partial n}\frac{\partial n}{\partial p} \tag{2.4}$$

Substituting Equation (2.2) for ϕ in Equation (2.4) leads to

$$\frac{d\phi}{dp} = \frac{4\pi n}{\lambda}\frac{\partial l}{\partial p} + \frac{4\pi l}{\lambda}\frac{\partial n}{\partial p} \tag{2.5}$$

Where ∂l is small change in the thickness and ∂n is a small change in refractive index. Equation (2.5) indicates that $\frac{d\phi}{dp}$ depends upon elasto-optics and elasto-mechanical properties of the spacer. It is assumed that the change in the refractive index Δn of PDMS because of ultrasound is very small compared to the change in its cavity thickness Δl. For acoustic detection, the change in the cavity thickness is the main source of phase shift. The change in the cavity spacing dl per unit pressure dp is written as

$$\frac{dl}{dp} = \frac{l}{E} \tag{2.6}$$

which is obtained by rearranging the expression of Young's modulus E in terms of $\frac{dl}{dp}$ [17]. From Equation (2.5) and Equation (2.6) the acoustic sensitivity S_A of the sensor is expressed as

$$S_A = \frac{4\pi n}{\lambda}\frac{l}{E} \tag{2.7}$$

Equation (2.7) shows that acoustic sensitivity is proportional to the thickness of the spacer and inversely proportional to Young's modulus.

2.1.3.4 Sensitivity of FPI sensor

The product of optical phase sensitivity S_0 from Equation (2.3) with acoustic sensitivity S_A from Equation (2.7), defines the overall sensitivity of sensor S. The sensitivity of the sensor is expressed as,

$$S = \frac{dI(\phi)}{dp} = \frac{dI(\phi)}{d\phi}\frac{d\phi}{dp} \tag{2.8}$$

$$S = \frac{dI(\phi)}{d\phi}\frac{4\pi n}{\lambda}\frac{l}{E} \tag{2.9}$$

For a sensor having a thicker spacer will have higher acoustic sensitivity but reduced acoustic bandwidth because the sensor starts responding to spatial averages of the stress over its sensitive region. That's why there is a trade-off between spacer thickness choice and material's optical and mechanical properties to achieve high overall sensitivity while keeping large acoustic bandwidth. Higher optical sensitivity can be achieved by just increasing mirror reflectivities.

2.2 Thin film pressure response

Properties of a thin film are commonly studied using the load-deflection method [18]. In this method, the deflection of a suspended membrane is studied under applied pressure. In our fiber tip sensor, where a thin film is fabricated on the tip of the fiber with some spacing between the thin film and the fiber tip, there is a need to know how much deflection this membrane might undergo under certainly applied pressure. The will help us in figuring out the thickness and size of the membrane is needed. For a clamped round shape thin film on the fiber tip, the deflection under uniform pressure P is given by,

$$filmDeflection = \frac{3(1-\nu^2)P}{16EL^3}r^4 \tag{2.10}$$

where P is pressure, L is film thickness, r is effective film radius, E is Young's Modulus, and ν is Poisson's ration, respectively. If an object is stretched or compressed in the direction of applied pressure, it will undergo contraction or extension in the direction perpendicular to the applied pressure. Poisson's ratio is the ratio between these two quantities. This Equation (2.10) is valid only when the deflection of the membrane is smaller than 30% of film thickness, and film thickness should not be more than 20% of the diameter of film. For any FPI sensor, its finite pressure measurement range depends upon its thickness and radius as well as E and μ value.

2.3 Measures of quality of Fabry-Perot Interferometer

2.3.1 Finesse

The measure of the quality of resonance of the interferometer is given by its finesse. Finesse is defined as the ratio of the Free Spectral Range (FSR) to the Full Width at Half Maximum (FWHM).

$$\mathfrak{f} = \frac{FSR}{FWHM} \tag{2.11}$$

The free spectral range is a frequency or wavelength spacing between adjacent resonances. The free spectral range in terms of wavelength is derived by equating the difference in phase between successive reflectance minima, which is 2π, with that for the derivative of the phase with respect to wavelength and rearranging to get the final expression,

$$FSR_\lambda = \frac{(\lambda_0)^2}{2nl} \tag{2.12}$$

where λ_0 is wavelength corresponding to first reflectance minima, n is the refractive index, and l is the length of the optical cavity. The cavity thickness and FSR have an inverse relation to each other. That means the smaller the cavity length larger the free spectral range (2.12).

2.3.2 Q-factor of optical resonator

Another parameter determining the performance of FPI is its Q-factor, which is defined as the ratio of energy loss per round trip to the initial energy stored in the resonant cavity. The Q-factor of FPI is defined as

$$Q = \frac{4\pi l}{\lambda_0 k} \tag{2.13}$$

where l is cavity thickness, λ_0 us wavelength at resonance and k is fractional power loss per round trip.

2.3.3 Visibility

Another important variable is visibility of the optical cavity, which is a measure of depth of reflectivity peaks in the transfer function. The visibility is defined as,

$$V = \frac{I_{max} - I_{min}}{I_{max} + I_{min}} \tag{2.14}$$

Where I_{max} and I_{min} are maximum reflected power and minimum reflected power in the reflection mode of ITF. For an ideal non-diverging, perfectly collimated beam, the visibility is 1.

2.4 Chapter Conclusions

The theory fundamentals on the extrinsic FPI has been explained. Now it is possible to understand how the sensor works and tests its performance for incident acoustic pressure waves. The operating principle of an FPI inside an optical fiber allows to have multiple cavities to monitor perturbations of different parameters (i.e., refractive index, temperature, etc.); in our case, our cavity is sensing incident ultrasound waves. The high sensitivity from the optical sensing devices makes this sensor an interesting alternative to detect acoustic signals with the advantages of optical fibers.
In Chapter 3, the method for fabricating fiber optic tip sensor using two different schemes is summarized. Each fabrication step is explained with full details to get a picture of the fabricated sensor.

Chapter 3

FPI Sensor Fabrication

This chapter describes the design of fiber tip sensor used for the experiment in this thesis to detect ultrasound signals. Detailed explanation of each fabrication steps are also mentioned in this section. This chapter includes the polymer material properties as well as the dielectric mirror properties used for fabricating the sensor

3.1 Sensor Designs

Two different sensor designs are proposed as Fiber-tip sensor. First design includes fabricating Fabry-Perot etalon directly onto the fiber tip itself, while second design introduces optical cavity using multi-mode fiber and chemical etching process to make a more flexible Fabry Perot cavity. The design of the fiber tip sensors are as follows:

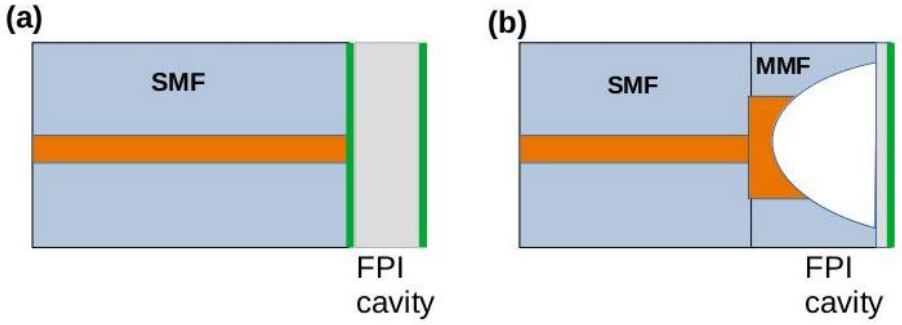

FIGURE 3.1: Design of the Fiber-tip sensor.(a)First sensor design (b)Second sensor design

3.2 Fabrication of fiber tip sensor

This section explains, the fabrication process of the sensors used for the experiment in this thesis.

3.2.1 First fabrication method

In this method, the polymer spacer is directly fabricated onto the single mode optical fiber (SMF) with silver reflective mirror coating on both side of the polymer spacer. The fabrication process of the sensor head includes steps as follows:
A 30cm length of 1550nm single mode optical fiber (outer diameter 125um and core diameter of 9um) is perpendicularly cleaved using mechanical fiber cleaver() , see Fig3.1(a). Then this cleaved fiber was cleaned and loaded into a mount of the dc sputtering system for the deposition of the reflective coating, as shown in Fig3.1(b). Thin silver films were used for the reflective coating, with optical reflectivity of the coating being controlled by the film thickness. The silver film thickness can be controlled by the sputtering power and duration of the sputtering. Finally to make a polymer spacer, commercially available polydimethylsiloxane(PDMS) (Sylgard 184) was used. The polymer precursor (Sylgard 184A) and curing agent (Sylgard 184B) was mixed in a ratio of 10:1 and degassed for 15 min in vacuum chamber to remove air bubbles.To make a very thin film of the PDMS a small amount of mixed polymer was spin coated on a glass substrate (4000rpm, for 1min). Through spin coating, a uniform PDMS film can be obtained with thickness ranging from 15-30 um. As shown in the Figure 3.2(c) after spreading PDMS polymer to obtain thin film this uncured PDMS was dip coated onto the fiber tip. This PDMS coated fiber tip was then put inside hot air oven for 4hr at 50^0C to thermally cure. After confirming that the PDMS was cured the fiber tip was again mounted inside dc sputtering system to deposit second silver reflective coating as shown in Figure 3.2(d). Figure 3.3 shows the microscopic images of the fabricated Fiber-tip sensor using the mentioned fabrication steps.

All the steps mentioned above are shown in the figure(3.2). The spacer thickness of the sensor fabricated above were observed to be 32um and 21um.

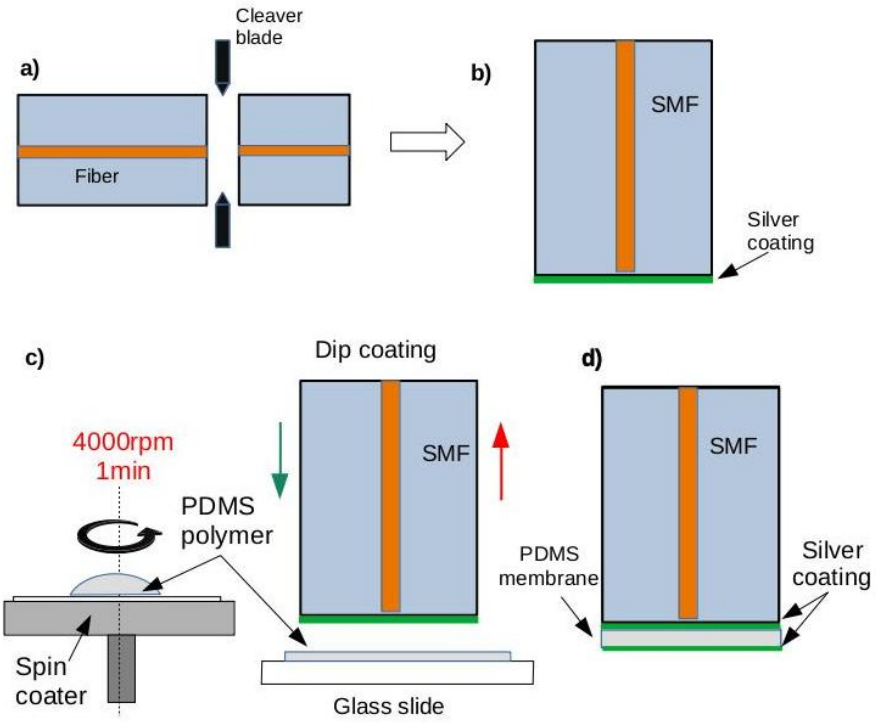

FIGURE 3.2: sensor fabrication steps (a)-(d), PDMS polymer spin coated on glass slide (c)

3.2.2 Second fabrication method

For the second proposed Fiber-tip sensor fabrication, the idea is to use to a chemically etched multi mode fiber (MMF) to connect the thin film and the fiber. The MMF is made up of same material as (SMF) with only difference being its core size is 64um. The fabrication process of the sensor are shown in Figure 3.4(a-f).

The protective plastic coating of the single mode fiber (SMF) was firstly removed and then the fiber was cleaved using the mechanical cleaver. The same process was done to the small piece of MMF. Afterward , this two fibers were spliced together using Fusion splicer(61s, Fujikura Ltd, Tokyo, Japan). This splicing of two fiber was carried out with fusion splicer being on its auto splicing mode setting. This spliced SMF and MMF was then fixed onto the mechanical cleaver with cleaving point being at 200um away from the spliced region. Then excessive MMF was cleaved away carefully only leaving 200um of the MMF splice with SMF as shown in Figure 3.4(c).Then as shown in Figure 3.4(d) this fiber was then submerged inside 49percent concentrated HF acid for etching purpose the 10min and then removed and cleaned with water. This process creates a 'U' shaped air cavity of around 60um depth. Next we again follow PDMS polymer (10:1 mixing ratio)

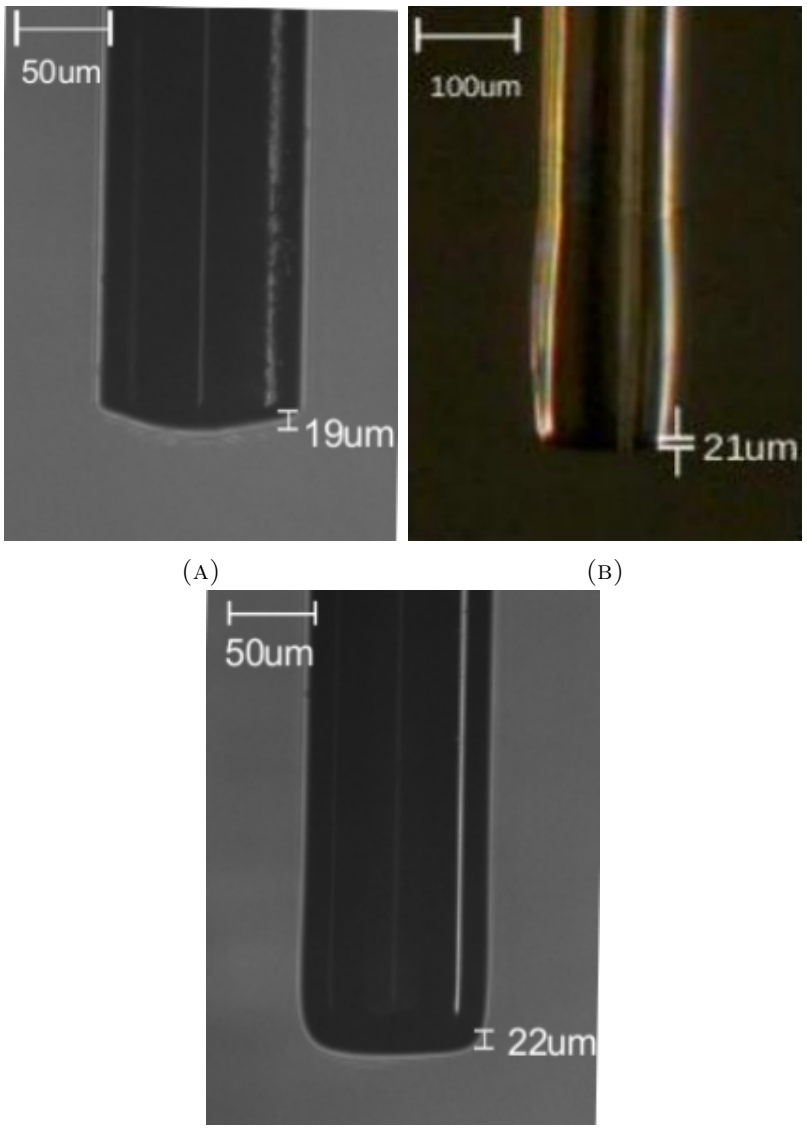

(A) (B)

(C)

FIGURE 3.3: Microscopic images of sensors using first fabrication method

mixing steps and spin coating it on the glass substrate to make 15-30um thin layer. The prepared fiber and PDMS coated glass slide is then fixed onto microscopic setup to dip coat the PDMS thin film onto fiber as shown in Figure 3.4(e). This dip coated fiber was then left inside hot air oven for 4hr at 50^0C for PDMS to be thermally cured. After confirming that PDMS was cured we load this fiber inside dc sputtering system to deposit silver mirror coating to increase overall reflectivity from fiber tip sensor as shown in Figure 3.4(f) Figure 3.5 shows the microscopic images of the fabricated Fiber-tip sensor using the mentioned fabrication steps. Microscopic setup and etching setup used during fabricating both sensor is shown in the Figure 3.6

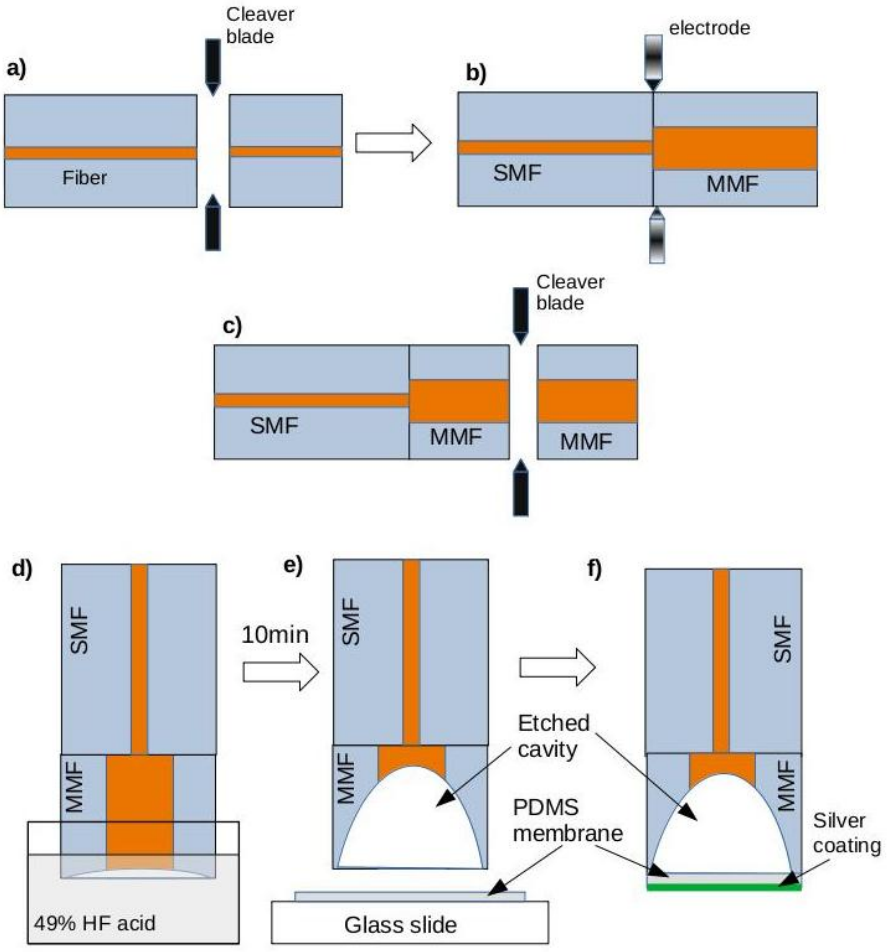

FIGURE 3.4: sensor fabrication steps (a)-(f), HF etching of fiber end (d), spin coated PDMS to be deposited on fiber tip, silver coating deposition on the cured PDMS membrane (f)

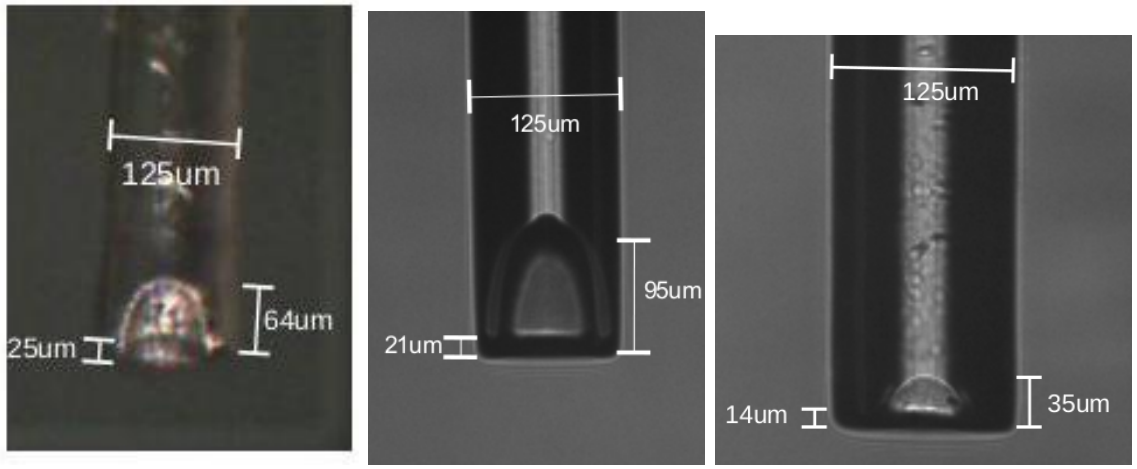

(A) (B) (C)

FIGURE 3.5: Microscopic images of sensors using second fabrication method

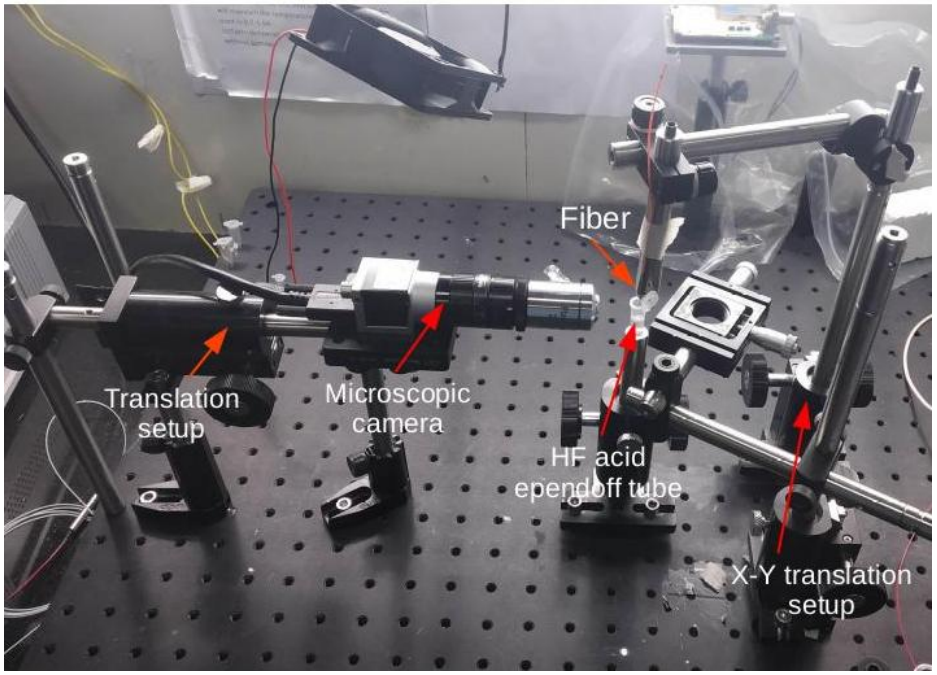

FIGURE 3.6: Microscopic and etching setup used during fabrication

Properties	**PDMS properties**
Young's modulus(MPa)	1.32
Refractive index	1.3997
Poisson ratio	o.5
Specific heat(kJ/kg K)	1.46
Water absorption (after 24hr)	0
Linear coefficient of thermal expansion at 25^0C(ppm)	309.63

TABLE 3.1: Mechanical and optical properties of PDMS

3.2.3 Properties of spacer layer and mirrors

3.2.3.1 Properties of spacer layer

Listed below are some properties of PDMS polymer [?]. PDMS is optically transparent with good dielectric properties. Also its water resistance makes it an excellent material to be used in sensor. Also PDMS film properties can be manipulated using elastomer

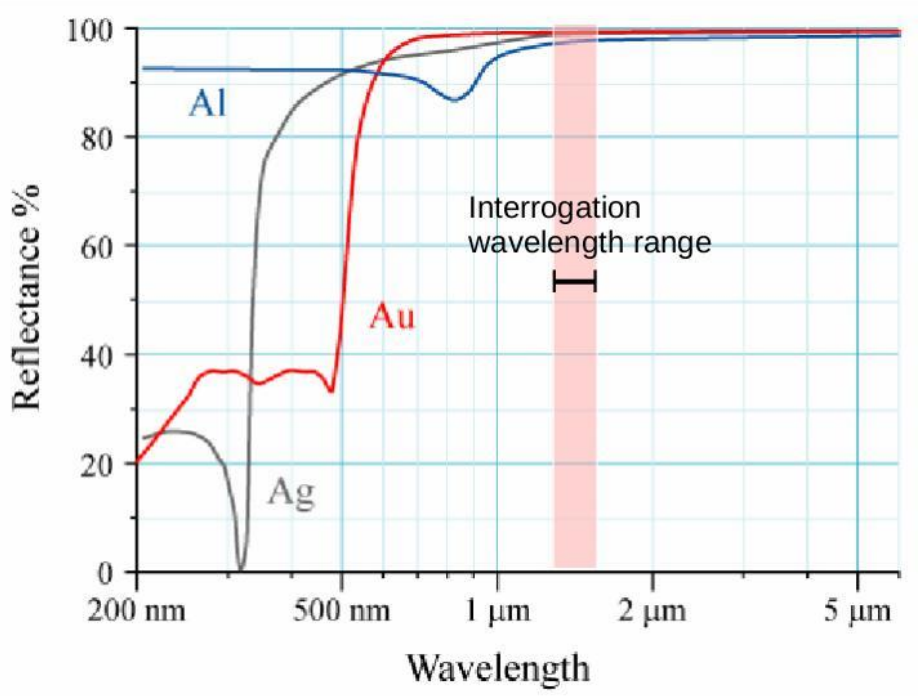

FIGURE 3.7: Comparison between reflection spectrum of dielectric mirrors forming FPI interferometric sensor

base and curing agent ratio and its curing temperature allowing us to make varied flexible membranes.

3.2.3.2 Dielectric mirror properties

The dielectric silver mirror on the both side of the polymer spacer forms the resonant cavity, with cavity thickness l. The dielectric mirror has very low optical adsorption, so the relation between the reflected power (R) and transmission power (T) is

$$R + T = 1 \tag{3.1}$$

where, absorption is very small and ignored. Figure 3.7 shows the comparison between the reflection spectrum of the gold, silver and aluminium mirrors. The silver mirrors are highly reflective between 1500nm - 1650nm, hence very low transmission. At this wavelength corresponding to telecoms bandwidth the FPI sensor is interrogated by robust and low cost semiconductor diode laser over with wide wavelength tuning range. Increasing mirror reflectivities in the region leads to increase in optical sensitivity for non diverging beam.

But for small beams sizes comparable to cavity thickness, this can cause the beam to diffract and can effect optical sensitivity.

3.3 Summary

This chapter has described the two sensor designs used in this thesis project. Also all the steps involving in the fabrication of this sensors are described with sufficient details. The microscopic images of the fabricated sensors are also shown for corresponding methods. The optical and mechanical properties of the polymer material used for making Fabry-Perot cavity has also been mentioned. The dielectric mirrors properties on the either side of the spacer cavity have also been summarised.

Chapter 4

Experimental Setup

This chapter details the experimental arrangements and results validating the fabricated flexible FPI sensor. Section 4.1 describes the experimental setup used to verify the ultrasound pressure field response of the FPI sensor. The pressure field is generated by an ultrasound piezoelectric transducer in the water.

4.1 Experimental schematic

The Schematic of the experimental setup is shown in Figure 4.1. The experimental system consists of ASE broadband optical source with wavelength ranging from 1528nm to 1568nm (Telecoms, C-band). The optical source output is connected to Port-1 of the three-port optical circulator (3dB isolation loss) with SMF optical fiber connecting end (Red). The FPI sensor is directly connected to the Port-2 of the optical circulator by means of splicing. The light reflected from the FPI sensor is circulated from Port-2 to Port-3 of the optical circulator and connected to a 1x4 fiber optic switch (FOS). This fiber optic switch is USB-powered and controlled using an application on the control PC. One of the output channel of the FOS is connected to connected to InGaAs photodiode(PD) (ThorLabs 800-1700 nm). The photodiode measures the light reflected from the sensor. Another of the output channels of the FOS is connected to a spectrum analyzer (Bristol-771 laser spectrum analyzer) to measure the spectral information of the FPI sensor. Another FOS channel is connected to a digital oscilloscope (Tektronics DPO

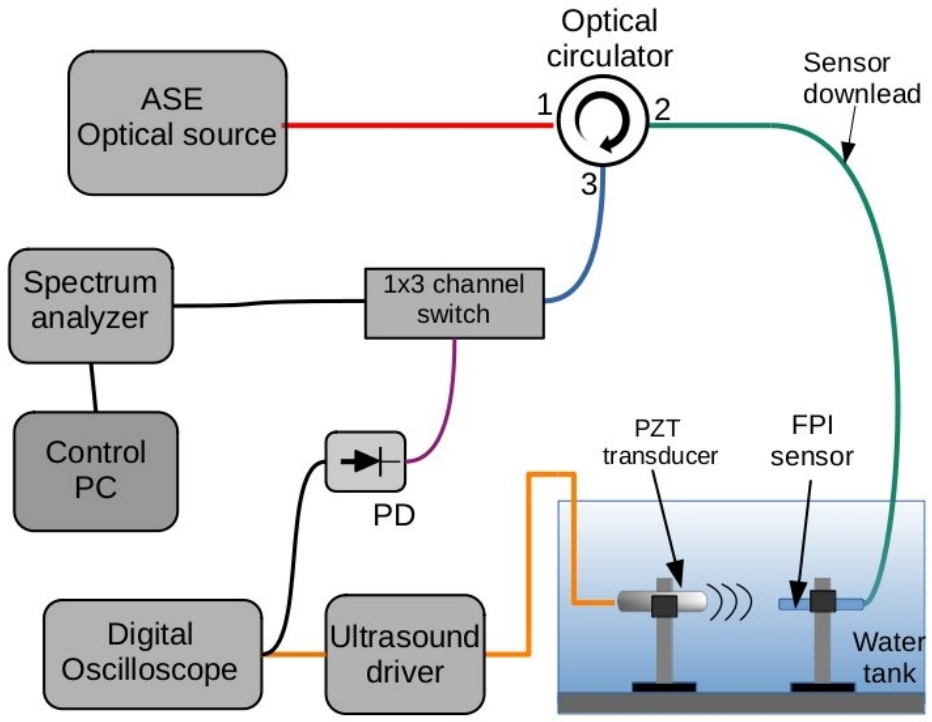

FIGURE 4.1: Schematic of the experimental setup used to interrogate the FPI sensor

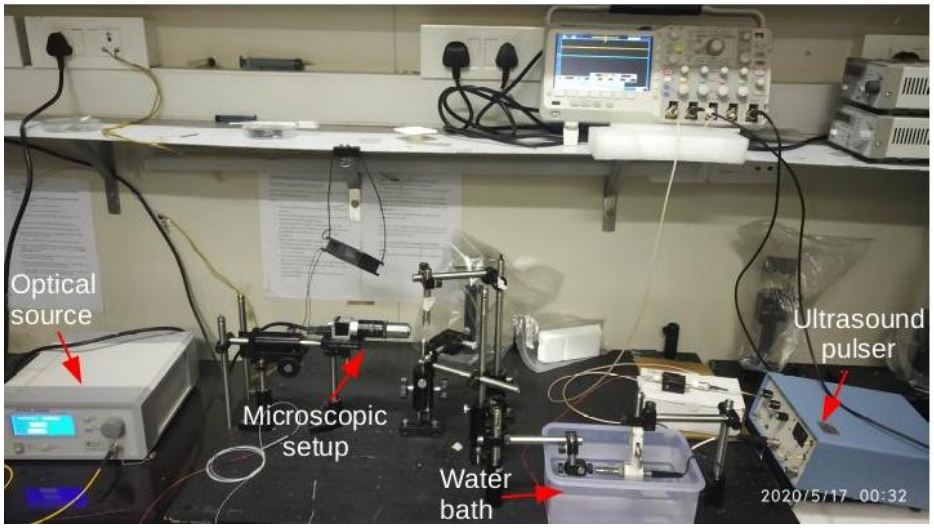

FIGURE 4.2: Actual experimental setup for ultrasound detection

2024B with the bandwidth of 200MHz and sampling rate 1Gs/S) for measuring the acoustic waveform. The ultrasound pressure field is generated using a commercially available ultrasound piezoelectric transducer (Olympus 5073 PR Pulsar / Receiver) in water. The sensor's frequency response is obtained by taking the Fourier transform of the recorded pulse response by the sensor.

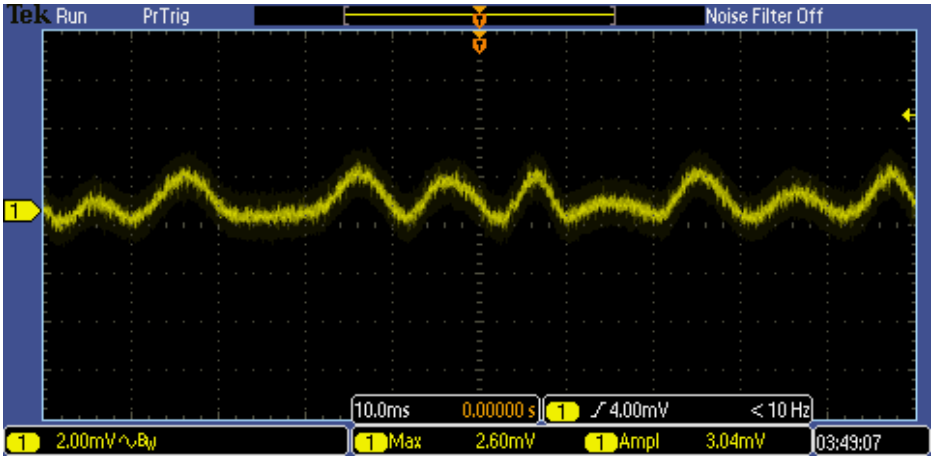

FIGURE 4.3: Time-domain frequency response from the FPI sensor

The PZT has a resonant frequency of 10 MHz and is powered by pulsar to produce an ultrasound pulse. Figure 4.2 shows the ultrasound generated pulse, which is measured by the same PZT transducer using its Receiver mode by placing the FPI sensor close to the PZT transducer acoustic focal distance (2cm). It is seen that the ultrasound pulse consists of a few cycles of the 10 MHz signal.

4.1.1 Testing of First sensor scheme

The ultrasound frequency response of the sensor fabricated using the first sensor scheme has been carried out. Sinusoidal variation in the reflected back optical fiber was observed for 3.3c. For a PDMS polymer interferometric cavity directly fabricated onto the fiber end face, in the time domain, the frequency response was observed as shown in Figure 4.3.
This potential(v) vs. time sinusoidal variation in the reflected optical power from the sensor tip was observed for sensor 3.3c and confirms the presence of the FPI cavity. After confirming the formation of an FPI cavity on the fiber tip, the sensor was tested for its ultrasound frequency response underwater using the above mentioned experimental arrangements. Figure 4.4 shows the sensors underwater tasting setup.
Figure 4.5 shows the ultrasound generated pulse, which is measured by the same PZT using "T/R" mode trough the end face of the fiber tip. The FPI sensor is placed near the focus of the transducer for maximum pressure amplitude. PZT transducer detects a reflected back signal 14μs later, which exactly where the fiber sensor tip is placed. No ultrasound response was observer from the fabricated sensor as of yet.

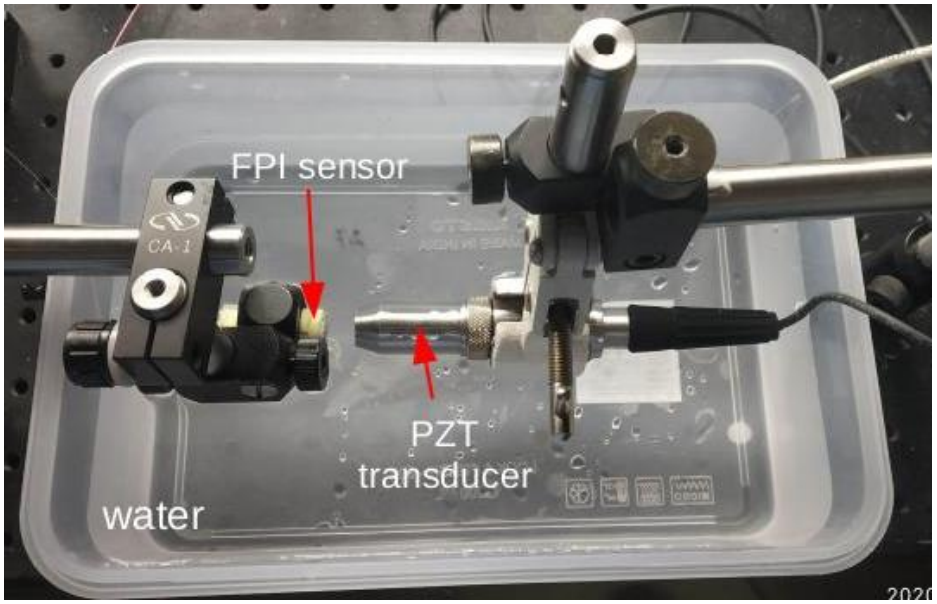

FIGURE 4.4: setup of underwater sensor testing

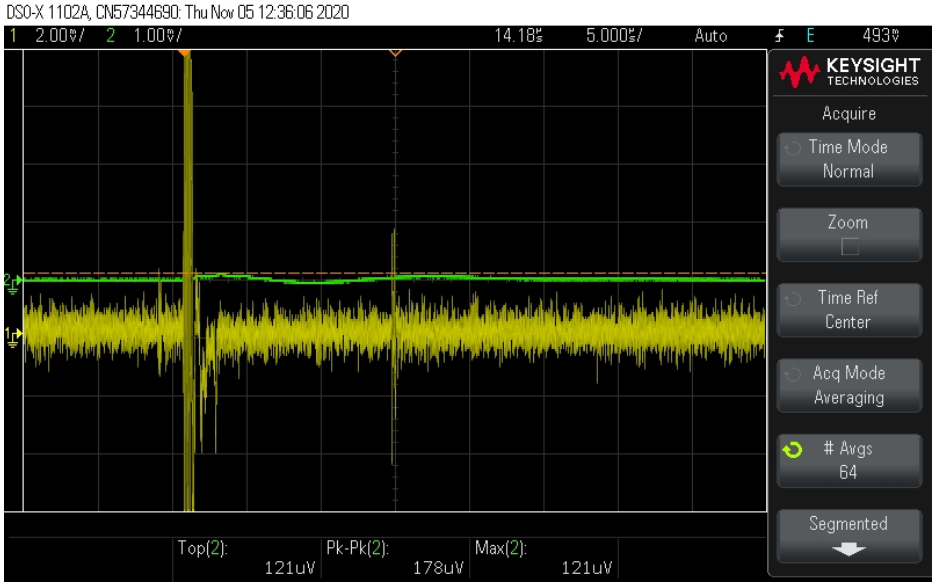

FIGURE 4.5: Frequency response test of FPI sensor, 'yellow' signal is from a pulse of 10-MHz PZT transducer and 'green' signal is response of fiber tip sensor.

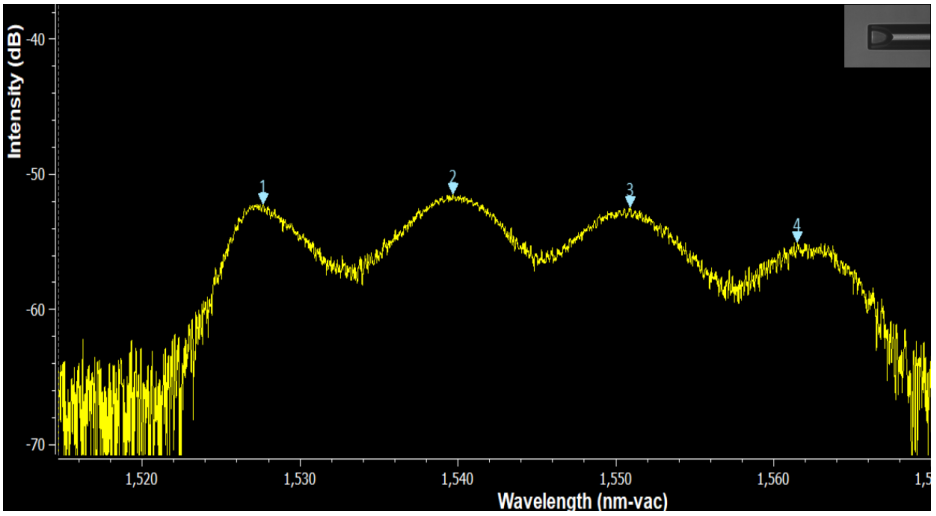

FIGURE 4.6: Reflection spectrum of fabricated FPI sensor using second fabrication scheme

4.1.2 Testing of Second sensor scheme

Figure 4.6 shows reflection spectrum of a sensor measured by spectrum analyzer (Bristol-771 laser spectrum analyzer). This sensor is fabricated using second proposed sensor scheme. This spectrum is a result of interference between laser light intensity reflected from the fiber-air interface and air-PDMS membrane with reflective optical coating on the PDMS membrane. The cavity length L can be calculated by

$$L = \frac{\lambda_1^2}{2n\delta\lambda} \tag{4.1}$$

where λ is the dip wavelength, n is refractive index of cavity and $\delta\lambda$ is the wavelength spacing between two adjacent fringes. The sinusoidal interference fringes indicates that the FPI cavity length is around 96.2um which is close to our observed cavity length 95um. Here the value of λ is selected at wavelength 1539.5nm.

Chapter 5

Conclusion and Future Work

5.1 Conclusion

1. Two unique fabrication methods for FPI tip sensors have been proposed and experimentally demonstrated. Methods such as spin coating, dip-coating, chemical etching are used to prepare both fiber and thin-films.

2. Proposed sensor design1 directly have thin polymer film fabricated on the end face of SMF. As for sensor design2, the prepared film is then transferred onto the fiber tip, which is made up of spliced SMF and MMF and cleaved to the desired length.

3. The fabrication method leads to very thin and controlled film thickness and many different polymer materials can be utilized for the film.

4. FPI cavity lengths have been measured using both mechanical methods and from spectral data for the cavity, the cavity spacing matched with small error.

5. The high-frequency response of the proposed sensors needs further testing to be done.

5.2 Future Work

1. The sensitivity and frequency response needs to be improved by using thinner films and cavity spacing with a smaller length.

2. Different materials, such as graphene, gelatin, UV-epoxy, and polyvinyl chloride (PVC) as a film could be studied for fabricating novel sensor designs.

3. Some special fiber can be used to get unique fiber tip sensors. For example, using fiber with a double-clad can accommodate a unique sensor design. Also, using germanium doped fiber for chemical etching leads to unique 'V" shaped etching, which is very useful for making non-diverging optical beams at the end of the fiber tip.

4. Most of the polymer materials used in fabricating sensors are temperature sensitive; their physical properties tend to change with a temperature shift change. So the effect of thermal expansion should be considered when designing the FPI tip sensor to improve their performance further.

5. For the sensing system, a low-noise photo-detection device with higher bandwidth is required for small details of the sample is to be detected. So just by improving the sensing system results in detection pressure signals with higher quality. Optical sensors' ability to detect pressure signals can be utilized for biomedical imaging if better signals are detected, with optical fiber's small size.

6. A numerical simulation of a Fabry-Perot cavity to observe the limits between which FPI cavity transducing the pressure changes correctly into phase changes is also required.

7. To improve the sensor's overall performance, a numerical simulation of the optical cavity for varying pressure fields and how it translates into shifts in wavelength is highly necessary. So doing a numerical simulation of the optical cavity beforehand will help tremendously in improving sensor performance.

5.3 Summary

Fabry Perot Interferometric polymer film ultrasound sensors can fulfill many requirements for measuring medical ultrasound fields. High sensitivity, wideband, and acoustically small sensor size that can self calibrate can be configured as 2D array for rapid field mapping applications or simply as miniature optical fiber hydrophones for in situ measurements. These sensors' low cost means they can be regarded as consumable that can be replaced

after one-time use or for measuring high intensity focused ultrasound field where there is a risk of damaging expensive PVDF hydrophones. To this date, bandwidths are limited to around 20MHz. Recently the use of high-frequency ultrasound is increasing because of ocular medicine and harmonic imaging, leading to the demand for large bandwidth sensors. So the future work will involve increasing the sensitivity of sensors and increasing the bandwidth as well. An increase in bandwidth is possible by reducing the polymer film thickness to less than $10um$ while retaining high sensitivity by increasing the finesse of FPI and the increase in the laser's power.

Bibliography

[1] D. H. Wang, P. G. Jia, S. J. Wang, C. L. Zhao, D. P. Zeng, H. Wang, and F. Q. Li. Tip-sensitive all-silica fiber-optic fabry–perot ultrasonic hydrophone for characterising high intensity focused ultrasound fields. *Applied Physics Letters*, 103(4):044102, 2013. doi: 10.1063/1.4816329. URL https://doi.org/10.1063/1.4816329.

[2] Jingjing Guo, Shigui Xue, Qun Zhao, and Changxi Yang. Ultrasonic imaging of seismic physical models using a phase-shifted fiber bragg grating. *Opt. Express*, 22 (16):19573–19580, Aug 2014. doi: 10.1364/OE.22.019573. URL http://www.opticsexpress.org/abstract.cfm?URI=oe-22-16-19573.

[3] Horacio Lamela, Daniel Gallego, and Alexander Oraevsky. Optoacoustic imaging using fiber-optic interferometric sensors. *Opt. Lett.*, 34(23):3695–3697, Dec 2009. doi: 10.1364/OL.34.003695. URL http://ol.osa.org/abstract.cfm?URI=ol-34-23-3695.

[4] Q. Rong, R. Zhou, Y. Hao, X. Yin, Z. Shao, T. Gang, and X. Qiao. Ultrasonic sensitivity-improved fabry–perot interferometer using acoustic focusing and its application for noncontact imaging. *IEEE Photonics Journal*, 9(3):1–11, June 2017. ISSN 1943-0655. doi: 10.1109/JPHOT.2017.2702719.

[5] B. Culshaw. Optical fiber sensor technologies: opportunities and-perhaps-pitfalls. *Journal of Lightwave Technology*, 22(1):39–50, Jan 2004. ISSN 1558-2213. doi: 10.1109/JLT.2003.822139.

[6] Lars Rindorf and Ole Bang. Sensitivity of photonic crystal fiber grating sensors: biosensing, refractive index, strain, and temperature sensing. *J. Opt. Soc. Am. B*, 25(3):310–324, Mar 2008. doi: 10.1364/JOSAB.25.000310. URL http://josab.osa.org/abstract.cfm?URI=josab-25-3-310.

[7] Pietro Ferraro and Giuseppe De Natale. On the possible use of optical fiber bragg gratings as strain sensors for geodynamical monitoring. *Optics and Lasers in Engineering*, 37(2):115 – 130, 2002. ISSN 0143-8166. doi: https://doi.org/10.1016/S0143-8166(01)00141-5. URL http://www.sciencedirect.com/science/article/pii/S0143816601001415. Optical Methods in Earth Sciences.

[8] Alan D. Kersey, Se For, and Alan D. Kers +a. Optical fiber sensors for permanent downwell monitoring applications in the oil and gas industry. 2000.

[9] Lutang Wang and Nian Fang. Applications of fiber-optic interferometry technology in sensor fields. 2017. doi: 10.5772/66276. URL https://doi.org/10.5772/66276.

[10] T. D. Fabry–perot interferometers: Cambridge studies in modern optics 3. (2): 319–320, 1986. doi: 10.1017/S0263034600001919.

[11] Temperature-insensitive miniaturized fiber inline fabry-perot interferometer for highly sensitive refractive index measurement. page 5764–5769, (2008). URL https://doi.org/10.1364/oe.16.005764.

[12] Mingzheng Jiang and Edmund Gerhard. A simple strain sensor using a thin film as a low-finesse fiber-optic fabry–perot interferometer. *Sensors and Actuators A: Physical*, 88(1):41 – 46, 2001. ISSN 0924-4247. doi: https://doi.org/10.1016/S0924-4247(00)00494-5. URL http://www.sciencedirect.com/science/article/pii/S0924424700004945.

[13] Alexander Graham Bell. On the production and reproduction of sound by light. *American Journal of Science*, s3-20(118):305–324, 1880. ISSN 0002-9599. doi: 10.2475/ajs.s3-20.118.305. URL https://www.ajsonline.org/content/s3-20/118/305.

[14] W. F. Cheong, S. A. Prahl, and A. J. Welch. A review of the optical properties of biological tissues. *IEEE Journal of Quantum Electronics*, 26(12):2166–2185, Dec 1990. ISSN 1558-1713. doi: 10.1109/3.64354.

[15] Robert A. Kruger. Photoacoustic ultrasound. *Medical Physics*, 21(1):127–131, 1994. doi: https://doi.org/10.1118/1.597367. URL https://aapm.onlinelibrary.wiley.com/doi/abs/10.1118/1.597367.

[16] E. Cibula, D. Donlagic, and C. Stropnik. Miniature fiber optic pressure sensor for medical applications. 1:711–714 vol.1, June 2002. doi: 10.1109/ICSENS.2002.1037190.

[17] P. C. Beard and T. N. Mills. Extrinsic optical-fiber ultrasound sensor using a thin polymer film as a low-finesse fabry-perot interferometer. *Applied Optics*, 35(4):663–675, August 1996. URL https://doi.org/10.1364/AO.35.000663.

[18] Osamu Tabata, Ken Kawahata, Susumu Sugiyama, and Isemi Igarashi. Mechanical property measurements of thin films using load-deflection of composite rectangular membranes. *Sensors and Actuators*, 20(1):135 – 141, 1989. ISSN 0250-6874. doi: https://doi.org/10.1016/0250-6874(89)87111-2. URL http://www.sciencedirect.com/science/article/pii/0250687489871112. A Special Issue Devoted to Micromechanics.